Extreme Mechanics of Probing the Ultimate Strength of Nanotwinned Diamond

Bing Li, Hong Sun, and Changfeng Chen

Phys. Rev. Lett. **117**, 116103 — Published 9 September 2016

DOI: 10.1103/PhysRevLett.117.116103

Extreme Mechanics of Probing the Ultimate Strength of Nanotwinned Diamond

Bing Li,[1,2] Hong Sun,[1,2,*] and Changfeng Chen[3,†]

[1]*Department of Physics and Astronomy and Key Laboratory of Artificial Structures and Quantum Control (Ministry of Education), Shanghai Jiao Tong University, Shanghai 200240, China*

[2]*Collaborative Innovation Center of Advanced Microstructures, Nanjing 210093, China*

[3]*Department of Physics and High Pressure Science and Engineering Center, University of Nevada, Las Vegas, Nevada 89154, USA*

(Dated: August 31, 2016)

Abstract

Recently synthesized nanotwinned diamond (nt-Dia) exhibits unprecedented Vickers hardness exceeding 200 GPa [*Nature* **510**, 250 (2014)]. This extraordinary finding challenges the prevailing understanding of material deformation and stress response under extreme loading conditions. Here we unveil by first-principles calculations a novel indenter-deformation generated stress confinement mechanism that suppresses the graphitization or bond collapse failure modes commonly known in strong covalent solids, leading to greatly enhanced peak stress and strain range in the indented diamond lattice. Moreover, the twin boundaries in nt-Dia promote a strong stress concentration that drives preferential bond realignments, producing a giant indentation strain stiffening. These results explain the exceptional indentation strength of nt-Dia and offer insights into the extreme mechanics of the intricate interplay of the indenter and indented crystal in probing ultrahard materials.

PACS numbers: 62.25.-g, 81.40.Jj, 61.50.Ah

Searching for materials harder and more stable than diamond has been an enduring quest driven by both practical needs and the fundamental desire to probe the ultimate limits of material strength. There have been extensive efforts exploring materials with different (than pure carbon) chemical compositions that exhibit high hardness and superior thermal stability. Notable examples include carbon nitrides, boron nitrides, and transition-metal borides [1–4]; but these materials fall short of reaching, let alone exceeding, the strength and hardness of diamond. Another approach achieves strength enhancement in materials by controlling their microstructural size, known as the Hall-Petch effect [5, 6], based on the idea that reducing grain (or twinning) size would suppress the nucleation and motion of dislocations by grain (twin) boundaries. This approach has produced remarkable results in nanostructured metals [7] and strong covalent solids like boron nitride [8] and diamond [9], turning them harder than their bulk counterparts. At further reduced grain (twin) sizes, however, an opposite phenomenon, known as the reverse Hall-Petch effect [10, 11], takes place when the usually weaker interactions at the grain (twin) boundaries dominate the plastic deformation process.

It was recently reported [12] that a nanotwined diamond (nt-Dia) structure exhibits unprecedented high Vickers indentation hardness exceeding 200 GPa, which is twice the commonly quoted hardness value of about 100 GPa for single-crystal cubic diamond. This result surpasses by a surprisingly large margin the hardness of all previously reported materials. More intriguing, this colossal hardness enhancement in nt-Dia cannot be explained by the Hall-Petch effect since the typical twin boundary (TB) separations ($\lambda = 3 \sim 6$ nm) in the synthesized nt-Dia are well inside the reverse Hall-Petch region (below about 10 nm), where the TB interactions are expected to dominate. To elucidate the unexpected strengthening of nt-Dia, it is essential to examine the structural and stress response to indentation loading.

In this work, we explore the extreme mechanics of probing the ultimate strength of nt-Dia. We employ first-principles calculations to examine the deformation and stress response of both the indenter and indented material under a variety of loading conditions. From calculated compressive stress data we set up a compressible Vickers indenter model to account for the large but finite normal stress beneath the indenter, which has been assumed to be unlimited (i.e., incompressible indenter) in past studies. This new indenter-deformation generated stress confinement prevents the graphitization or bond collapse failure modes commonly known for strong covalent solids, leading to greatly enhanced peak stress and strain

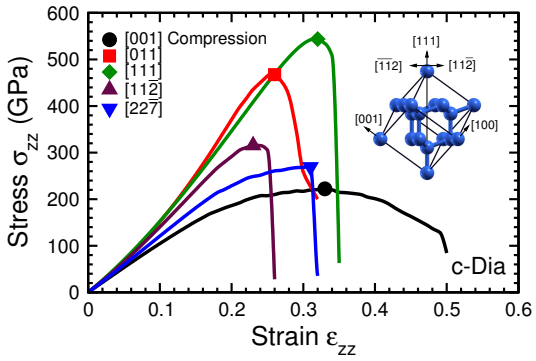

FIG. 1: (Color online) Calculated stress-strain relations of cubic diamond compressed along various directions.

range compared to those obtained from the incompressible indenter model. Moreover, we have identified a robust mechanism for bond realignment stemming from a TB-induced stress concentration, which produces a giant indentation strain stiffening in nt-Dia. These results explain the unprecedented high strength and hardness of nt-Dia, and the insights into the novel structural deformation and strengthening mechanisms advance the fundamental understanding of material behavior under extreme indentation loading conditions.

Stress-strain relations from first-principles calculations provide an accurate description of material deformation and strength [13–23], and the results can be directly compared to well-controlled nanoindentation measurements [24–26]. Under indentation, shear instability usually precedes the initiation of cracks and dislocations [27], signaling the onset of incipient plasticity [16, 18], and bond collapse may also occur under a compressive stress [28]. To determine the indentation strength, calculations were carried out under a biaxial stress field that contains a shear (σ_{zx}) and a normal compressive (σ_{zz}) stress component that obey the relation $\sigma_{zz} = \sigma_{zx} tan\phi$, where ϕ is the centerline-to-face angle of the indenter [28]. Here the diamond indenter is assumed to be incompressible and, therefore, the two stress components are always proportional to each other, which is a good approximation for most materials, including those with strengths comparable to that of cubic diamond [29, 30]. We will show below, however, that when the indented material is much stronger than cubic diamond, as in the case of nt-Dia, the deformation-limited finite peak strength of the diamond indenter has a major influence on the deformation modes and stress response of the indented material and must be explicitly considered.

The pyramid faces of the Vickers indenter are formed by the diamond $\{22\bar{7}\}$ crystalline

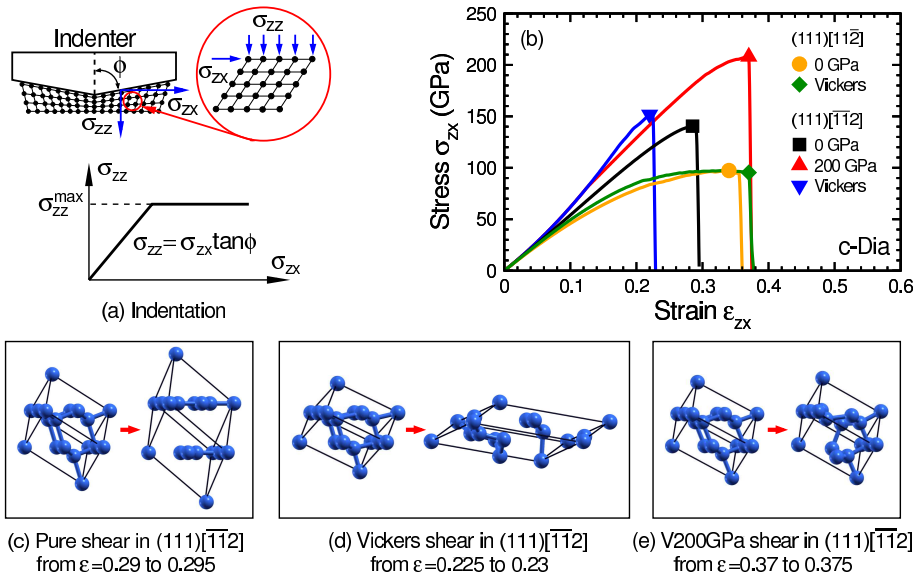

FIG. 2: (Color online) (a) A sketch of indentation stress conditions and the relation between the shear stress σ_{zx} and normal stress σ_{zz} beneath the indenter. (b) Calculated stress-strain relations of cubic diamond in the easy ((111)[11$\bar{2}$]) and hard ((111)[$\bar{1}\bar{1}$2]) directions under pure shear ($\sigma_{zz}^{max} = 0$), constrained shear ($\sigma_{zz}^{max} = 200$ GPa), and Vickers shear. Also shown are the snapshots of cubic diamond deformed in the hard ((111)[$\bar{1}\bar{1}$2]) direction right before and after (c) graphitization under pure shear, (d) bond collapse under Vickers shear, and (e) a new bond breaking mode under the constrained (V200GPa) shear.

planes meeting at the indenter tip with a centerline-to-face angle of $\phi = 68°$, and these planes arrange in a composite direction along the [001] axis [31]. We have employed first-principles calculations [32] to determine the stress-strain relations of diamond under compression, and the results (Fig. 1) are direction dependent. In the [001] direction, the peak compressive stress is about 200 GPa, while in the $\{22\bar{7}\}$ direction it is about 270 GPa. These peak stresses are much higher than the shear strengths of most indented materials and can be practically regarded as unlimited (i.e., incompressible) in holding the relation $\sigma_{zz} = \sigma_{zx} tan\phi$. For extremely ultrahard materials like nt-Dia, however, this relation must be modified to account for the diamond indenter's finite peak compressive stress. Here we propose a model relation,

$$\sigma_{zz} = \begin{cases} \sigma_{zx} tan\phi & \text{for } \sigma_{zz} \leq \sigma_{zz}^{max} \\ \\ \sigma_{zz}^{max} & \text{otherwise,} \end{cases}$$

where σ_{zz}^{max} is the maximum normal stress produced by the indenter. When $\sigma_{zz}^{max} = 0$, this relation describes the pure shear process considered in previous studies [13–21, 23]. In the opposite limit of $\sigma_{zz}^{max} \to \infty$, the normal stress is always proportional to the shear stress [28, 30]. Here, we examine a compressible indenter that has a large but finite peak normal stress σ_{zz}^{max}. As σ_{zx} (or σ_{zz}) is small, we can neglect the contacting friction between the indenter and indented nt-Dia and assume a linear relation $\sigma_{zz} = \sigma_{zx} tan\phi$ so that the resultant force is orthogonal to the boundary between indenter and nt-Dia; and as σ_{zx} (or σ_{zz}) becomes large, the strong normal pressure can deform the indenter to increase the contacting friction at the boundary between the indenter and nt-Dia and reduce σ_{zz} smoothly to a constant σ_{zz}^{max}. While the abrupt switch from the linear relation to the constant maximum normal stress is approximate, this model relation captures the main physics at both small strains, where the linear relation is accurate, and at large strains, where the normal stress reaches the (constant) maximum value, and the present formulism covers the intermediate strains by a simple interpolation that is easy to implement in computation. Our calculations unveil a new deformation mechanism under a compressible indenter that produces a giant strength enhancement, and this mechanism is insensitive to the model details and remains robust over a wide range of σ_{zz}^{max}. Below we concentrate on the representative case of $\sigma_{zz}^{max} = 200$ GPa, which is the peak stress in the composite [001] direction of the Vickers indenter.

The strongly directional carbon bonds in diamond produce highly anisotropic stress response. To unveil the extraordinary indentation strength of nt-Dia, it is instructive to first examine the stress-strain relations of diamond under various loading conditions. We show in Fig. 2 the calculated stress response of diamond to shear strains in its easy cleavage (111) plane along the easy ((111)[11$\bar{2}$]) and hard ((111)[$\bar{1}\bar{1}$2]) shear directions with $\sigma_{zz}^{max} = 0$ (pure shear), $\sigma_{zz}^{max} = 200$ GPa (the compressible Vickers indenter), and $\sigma_{zz}^{max} \to \infty$ (the incompressible Vickers indenter). The stress-strain curves for the two limiting cases (i.e., the pure shear and incompressible Vickers indentation) in the easy ((111)[11$\bar{2}$]) direction are nearly identical, and more detailed calculations (Fig. S1 [33]) show that the results for compressible Vickers indentation follow the same pattern. In contrast, the peak stress in

the hard ((111)[$\overline{1}\overline{1}$2]) direction depends on the loading condition. For $\sigma_{zz}^{max} = 0$ or $\rightarrow \infty$, the peak shear stress is about the same around 150 GPa, although they have different strain ranges; meanwhile, for $\sigma_{zz}^{max} = 200$ GPa, the peak shear stress is markedly increased to over 200 GPa with a much enhanced strain range. Similarly large peak shear stresses around 200 GPa are also obtained for σ_{zz}^{max} in a large range of 150 GPa - 300 GPa (Fig. S1 [33]), demonstrating the robustness of this striking phenomenon. To elucidate the underlying mechanism, we analyze the associated atomistic deformation modes.

When deformed in the hard ((111)[$\overline{1}\overline{1}$2]) shear direction in the two limiting cases, diamond undergoes two structural failure modes commonly known to occur in strong covalent solids [13–23, 28]: graphitization under $\sigma_{zz}^{max} = 0$ [Fig. 2(c)] and bond collapse under $\sigma_{zz}^{max} \rightarrow \infty$ [Fig. 2(d)]. Under the compressible Vickers indentation, however, the normal compressive stress is sufficiently strong to suppress the volume expansion associated with the graphitization yet limited to avoid the bond collapse in the normal [111] direction. As a result, none of the two common failure modes would occur; instead, the diamond crystal maintains its sp^3 bonding configuration until a new bond breaking mode occurs at a considerably expanded shear strain with a greatly enhanced peak stress exceeding 200 GPa [Fig. 2(b,e)]. This mechanism stems from the fundamental character of the carbon bond in the diamond structure and its response to the confined stress conditions, and it is insensitive to the details of the compressible indenter model as shown by the above calculated results (see Fig. 2(b) and Fig. S1 [33]). For single-crystal cubic diamond, the indentation strength is determined by its weakest link, namely the peak stress (about 100 GPa) in the easy shear direction, which is consistent with the measured Vickers hardness of diamond. In contrast, as shown below, the twin boundaries in nt-Dia promote a strong stress concentration under indentation loading, leading to bond realignments that transform the crystal structure into the hard shear direction in multiple mutually opposing directions, leaving no weak shear directions in the easy cleavage plane thus producing greatly enhanced strength.

We have modeled nt-Dia using a supercell containing nine C-C bilayers between neighboring TBs (nt-Dia-9), which has a TB separation of λ=1.84 nm [Fig. 3(a)]. We also have constructed a supercell twice as large (nt-Dia-18) and obtained similar results [33], and in the following we mainly focus on the nt-Dia-9 structure for a systematic examination. The calculated stress-strain curves of nt-Dia-9 under tensile or various shear deformation modes are shown in Fig. 3 (b,c) with the key structural snapshots presented in Fig. 3(d,e,f).

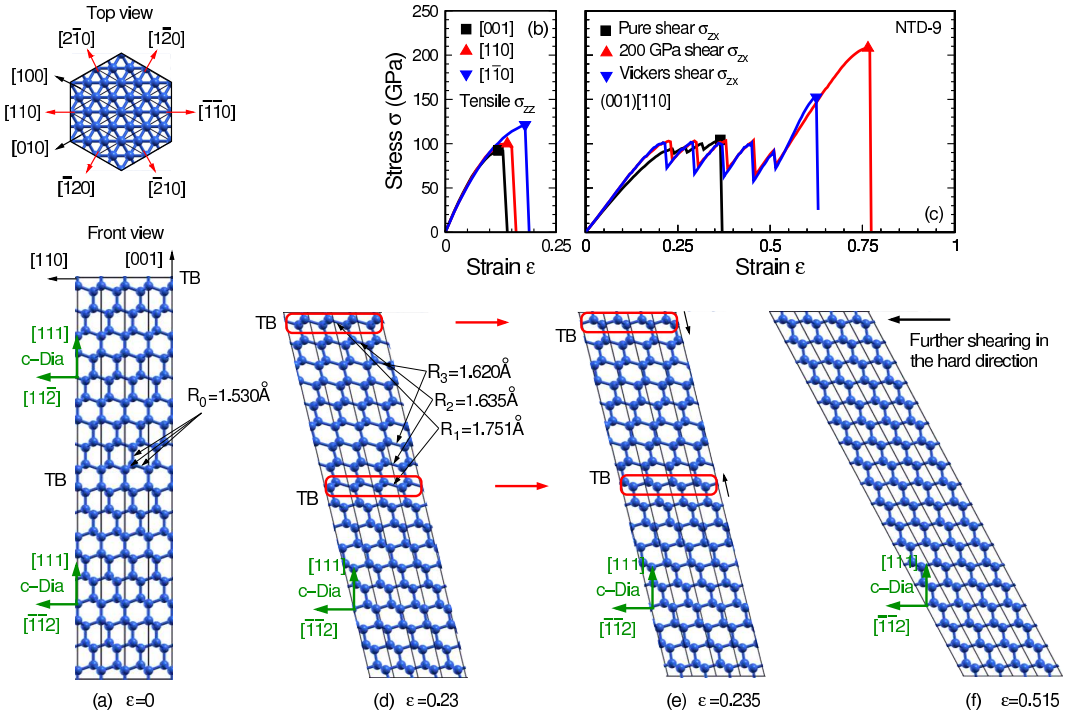

FIG. 3: (Color online) (a) The top and front view of the nt-Dia-9 unit cell at equilibrium ($\epsilon = 0$). The red and black arrows indicate various crystalline directions in nt-Dia-9, while the green arrows show the equivalent directions in cubic diamond. (b,c) Calculated stress-strain curves of nt-Dia-9 under various tensile directions and the indentation shear deformation in the (001)[110] direction with $\sigma_{zz}^{max} = 0$ (pure shear), $\sigma_{zz}^{max} = 200$ GPa (compressible Vickers indentation), and $\sigma_{zz}^{max} \to \infty$ (incompressible Vickers indentation). (d,e,f) Structural snapshots of nt-Dia-9 under compressible Vickers indentation in the (001)[110] shear direction at $\epsilon = 0.23$ and 0.235 right before and after the initial twin boundary movement by one atomic layer and at $\epsilon = 0.515$ when all the C-C bonds are aligned in the hard shear direction.

The tensile stress-strain results [Fig. 3(b)] indicate that the (001) planes of nt-Dia-9 are the dominant easy cleavage planes since they have the lowest peak tensile stress, and the (110) planes with a slightly higher peak tensile stress are also viable cleavage planes. We evaluate the indentation strength on these planes where indentation tests are performed. We first examine the results on the main cleavage (001) plane, which is equivalent to the diamond (111) plane. The calculated peak stress of nt-Dia-9 under pure shear ($\sigma_{zz}^{max} = 0$) is about 100 GPa, which is the same as that of single-crystal cubic diamond, thus showing no nanotwinning strength enhancement. Under the incompressible Vickers indentation model

($\sigma_{zz}^{max} \to \infty$), the peak stress increases markedly to about 150 GPa, but it is still considerably lower than the observed Vickers indentation hardness of 200 GPa [12]. Remarkably, under the compressible Vickers indentation model with $\sigma_{zz}^{max} = 200$ GPa the peak stress reaches a record high value exceeding 200 GPa, and it remains robust for a wide range of $\sigma_{zz}^{max} = 150$ to 300 GPa (Fig. S2 [33]). This result explains the experimental measurements [12], but the underlying mechanism requires further analysis.

The stress-strain curves under incompressible or compressible Vickers indentation both show a distinct saw-tooth pattern, which is attributed to bond rearrangements near the TBs. To illustrate this process, we show in Fig. 3 (d-f) a series of structural snapshots of nt-Dia-9 under the (001)[110] compressible Vickers indentation. The TB divides the structure into two parts with one (upper) half of the unit cell deformed in the easy shear direction and the other half in the hard shear direction. Consequently, the bonds are more stretched in the former with the most stretched bonds (R1) right next to the TB where the two halves meet. Such a TB-induced bond stretching pattern plays a key role in the indentation shear process in nt-Dia. At increasing strains, the most stretched bond (R1) flips and rebonds in such a way that it turns the atomic layer right next to the TB from the easy direction into the hard direction (see the atomic layers enclosed by the red boxes in Fig. 3d,e). The rebonding moves the TB by one atomic layer (Fig. 3e), and this process repeats itself and continues until all the carbon layers in the upper half of nt-cDia-9 are turned into the hard-direction alignment. As each bond flip occurs, the release of strain energy leads to a drop in the stress, producing the saw-tooth pattern in Fig. 3c. Once the bond realignment process is complete, the entire structure deforms in the hard shear direction under further indentation (Fig. 3f), and the stress response (Fig. 3c) becomes essentially identical to that of cubic diamond in its hard direction (Fig. 2b). In both cases, the large but limited normal stress beneath the compressible indenter prevents the graphitization or bond collapse modes, producing the larger strain range and giant strength enhancement.

There are three pairs of equivalent shear directions in the (001) easy cleavage plane of nt-Dia as indicated by the red arrows in Fig. 3(a): [110] ($[\overline{1}\overline{1}0]$), $[\overline{2}10]$ ($[2\overline{1}0]$), and $[1\overline{2}0]$ ($[\overline{1}20]$), which are evenly separated and mutually opposing. Under the indentation shear along each direction, the structure transforms into the hard shear direction via the TB-driven bond realignment mechanism discussed above, leaving no weak shear directions in the cleavage plane and making the structure highly resistant to indenter penetration. This is in stark

contrast to the situation for the (111) easy cleavage plane of cubic diamond, where the easy and hard shear directions are aligned directly opposite to each other [14, 21, 22], allowing the structure to deform along the easy shear direction despite the presence of the much harder (opposing) direction, thus limiting the indentation strength to about 100 GPa. The distinct structural arrangement in nt-Dia anchored by the TBs plays an essential role in promoting the stress concentration and bond realignment leading to the giant strength enhancement.

To further verify the robustness of the indenter-deformation generated stress confinement mechanism for strength enhancement in nt-Dia, we have performed extensive calculations to examine nt-Dia structures containing different number (up to four), type (regular and defective TBs), and size (nt-Dia-18, which has the TB separation of $\lambda = 3.67$ nm close to the experimental value of $\lambda = 3 \sim 6$ nm [12]) of TBs under the (001)[110] indentation shear strains. The obtained stress response and indentation strength enhancement (Fig. S3 [33]) are practically identical to those presented in Fig. 3. We also have performed calculations for nt-Dia-18 in another viable cleavage plane under the (110)[001] indentation shear, and the results (Fig. S4 [33]) show the same stress response pattern and enhanced peak stress over 200 GPa.

In summary, we have identified a novel mechanism for the unprecedented indentation strength in nt-Dia. An indenter-deformation generated stress confinement produces distinct deformation modes that are different than those obtained under pure shear or the previously used incompressible indenter model. The strong but limited normal stress beneath the compressible indenter produces much enhanced shear strain and indentation strength. The twin boundaries in nt-Dia play a crucial role in promoting a large stress concentration that drives systematic bond transformations to align the entire crystal in the hard shear direction. Such extreme mechanics underlie the highly unusual bonding change and the associated stress response in nt-Dia. These insights expand the fundamental understanding of structural deformation in both the indenter and indented crystal under extreme loading conditions, and the present results also provide guidelines and constraints for large-scale simulations of stress response and plasticity in ultrahard materials.

This work was supported by the NNSF and MOST of China (No. 11574197, No. 2016YFA0300500) at SJTU and by DOE under Cooperative Agreement No. DE-NA0001982 at UNLV. Computation was performed at the Center for High Performance Computing, Shanghai Jiao Tong University.

* Email:hsun@sjtu.edu.cn

† Email:chen@physics.unlv.edu

[1] A. Y. Liu and M. L. Cohen, Science **245**, 841 (1989).

[2] D. M. Teter and R. J. Hemley, Science **271**, 53 (1996).

[3] V. V. Brazhkin, A. G. Lyapin, and R. J. Hemley, Phil. Mag. A **82**, 231 (2002).

[4] R. B. Kaner, J. J. Gilman, and S. H. Tolbert, Science **308**, 1268 (2005).

[5] E. O. Hall, Proc. Phys. Soc. Lond. **64**, 747 (1951).

[6] N. J. Petch, J. Iron Steel Inst. **174**, 25 (1953).

[7] L. Lu, X. Chen, X. Huang, and K. Lu, Science **323**, 607 (2009); L. Lu, Y. Shen, X. Chen, L. Qian, and K. Lu, Science **304**, 422 (2004).

[8] V. L. Solozhenko, O. O. Kurakevych, and Y. Le Godec, Adv. Mater. **24**, 1540 (2012); N. Dubrovinskaia, *et al.* Appl. Phys. Lett. **90**, 101912 (2007).

[9] K. Tanigaki, *et al.* Nat. Commun. **4**, 2343 (2013).

[10] S. Yip, Nature **391**, 532 (1998).

[11] I. N. Remediakis, G. Kopidakis, and P. C. Kelires, IUTAM Book Series **13**, 171 (2009).

[12] Q. Huang, *et al.*, Nature **510**, 250 (2014).

[13] R. H. Telling, C. J. Pickard, M. C. Payne, and J. E. Field, Phys. Rev. Lett. **84**, 5160 (2000).

[14] H. Chacham and L. Kleinman, Phys. Rev. Lett. **85**, 85, 4904 (2000).

[15] S. H. Jhi, S. G. Louie, M. L. Cohen, and J. W. Morris, Jr., Phys. Rev. Lett. **87**, 075503 (2001).

[16] S. Ogata, J. Li, and S. Yip, Science **298**, 807 (2002).

[17] D. M. Clatterbuck, C. R. Krenn, M. L. Cohen, and J. W. Morris, Jr., Phys. Rev. Lett. **91**, 135501 (2003).

[18] S. Ogata,J. Li, N. Hirosaki, Y. Shibutani, and S. Yip, Phys. Rev. B **70**, 104104 (2004).

[19] X. Blase, P. Gillet, A. San Miguel, and P. Melinon, Phys. Rev. Lett. **92**, 215505 (2004).

[20] Y. Zhang, H. Sun, C. F. Chen, Phys. Rev. lett. **93**, 195504 (2004).

[21] Y. Zhang, H. Sun, and C. F. Chen, Phys. Rev. Lett. **94**, 145505 (2005).

[22] Y. Zhang, H. Sun, and C. F. Chen, Phys. Rev. B **73**, 144115 (2006).

[23] M. G. Fyta, I. N. Remediakis, P. C. Kelires, and D. A. Papaconstantopoulos, Phys. Rev. Lett. **96**, 185503 (2006).

[24] C. R. Krenn, D. Roundy, Marvin L. Cohen, D. C. Chrzan, and J. W. Morris, Jr., Phys. Rev. B **65**, 134111 (2002).

[25] M. I. Eremets, I. A. Trojan, P. Gwaze, J. Huth, R. Boehler, and V. D. Blank, Appl. Phys. Lett. **87**, 141902 (2005).

[26] T. Li, J. W. Morris, Jr., N. Nagasako, S. Kuramoto, and D. C. Chrzan, Phys. Rev. Lett. **98**, 105503 (2007).

[27] A. Gouldstone, H. J. Koh, K. Y. Zeng, A. E. Giannakopoulos, and S. Suresh, Acta. Mater. **48**, 2277 (2000).

[28] Z. C. Pan, H. Sun, and C. F. Chen, Phys. Rev. Lett. **98**, 135505 (2007).

[29] Y. Tian, *et. al.*, Nature **493**, 385 (2013).

[30] B. Li, H. Sun, and C. F. Chen, Nat. Commun. **5**, 4965 (2014).

[31] S. Takagi and T. Ishibashi, IMEKO 2010 TC3, TC5 and TC22 Conferences, Metrology in Modern Context, November 22-25, 2010, Pattaya, Chonburi, Thailand.

[32] Our calculations were performed using the VASP code (See http://www.vasp.at/), adopting the projector augmented wave (PAW) potentials [34], the local-density-approximation (LDA) with the exchange-correlation functional of Ceperley and Alder [35] as parametrized by Perdew and Zunger [36], and a plane-wave basis set. A 500 eV energy cutoff and a $10 \times 10 \times 2$ and $10 \times 10 \times 1$ Monkhorst-Pack k-point grid [37] were used for nt-Dia-9 and nt-Dia-18 with their unit cells given in Fig. 3(a) and Fig. S4(a) (a $10 \times 10 \times 10$ k-point grid is used for diamond with the unit cell given in the inset of Fig. 1). The energy, stress, and force convergence are 1 meV per atom, 0.1 GPa and 0.001 eVÅ^{-1}, respectively.

[33] See Supplemental Material at http://link.aps.org/ for details on calculated stress response of cubic diamond and various nt-Dia structures under a variety of loading conditions.

[34] G. Kresse and J. Joubert, Phys. Rev. B **59**, 1758 (1999).

[35] D. M. Ceperley and B. J. Alder, Phys. Rev. Lett. **45**, 566 (1980).

[36] J. P. Perdew and Y. Wang, Phys. Rev. B **45**, 13244 (1992).

[37] H. J. Monkhorst and J. D. Pack, Phys. Rev. B **13**, 5188 (1976).